INTERNATIONAL JOURNAL FOR NUMERICAL METHODS IN FLUIDS, VOL. 10, 591–602 (1990)

AN IMPROVED SIP SCHEME FOR NUMERICAL SOLUTIONS OF TRANSONIC STREAMFUNCTION EQUATIONS

WANG BAO-GUO AND CHEN NAI-XING

Institute of Engineering Thermophysics, Chinese Academy of Sciences, P.O. Box 2706, Beijing 100080, People's Republic of China

SUMMARY

A new improved strongly implicit procedure (SIP) is presented for solving large sets of transonic streamfunction equations with matrix of coefficients [**B**]. This algorithm has several advantages over those now in use. First, Stone's auxiliary matrix [**B**′] is non-symmetric, while in the present scheme the auxiliary matrix [$\tilde{\mathbf{B}}$] is symmetric and the matrix [$\mathbf{B} + \tilde{\mathbf{B}}$] is positive definite and symmetric when [**B**] is a symmetric matrix. This ensures the numerical stability of the iterative algorithms. Secondly, for an appropriate choice of iterative parameter ω, the rate of convergence of the new iterative procedure should be faster than the original SIP scheme.

Numerical results of the blade-to-blade flows are given with the present scheme. It is shown that the algorithm is efficient and robust.

KEY WORDS Shock capturing Streamfunction equation SIP scheme Finite difference Transonic cascade flow Comparison with experiment

INTRODUCTION

The most commonly used methods solve the transonic flow equations with either a time-dependent formulation or a time-like relaxation procedure. In general their convergence to a steady state solution is costly in time steps. Other methods have been devised to solve the steady flow problem directly as a large implicit system so that signals are felt at all points simultaneously. A difference equation is written for each grid point and the resulting set of simultaneous equations must be solved by using direct or some iterative means. In the present paper the transonic streamfunction equation for the steady relative flow problem is solved by the use of artificial compressibility. A new improved SIP scheme is used in numerical solutions of this set of equations.

STREAMFUNCTION EQUATION AND ARTIFICIAL COMPRESSIBILITY

In the present study the fluid is assumed to be an inviscid perfect gas. The flow is steady. Fluid velocities are taken relative to a rotating relative co-ordinate system (x^3, x^2, x^1) which has constant angular velocity relative to the inertial and absolute cylindrical co-ordinate system (r, ϕ, z). The (x^3, x^2, x^1) co-ordinate system used is shown in Figure 1. The x^3-co-ordinate is in the streamwise direction while x^2 is in the circumferential direction. To calculate the flow along the blade-to-blade surface, it is convenient to take co-ordinates (x^3, x^2) on the surface and x^1 normal

0271–2091/90/050591–12$06.00

Received May 1989
Revised August 1989

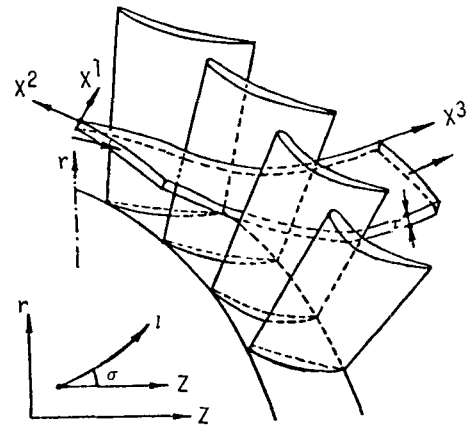

Figure 1. Curvilinear co-ordinates on blade-to-blade surface

to the surface. Then the fundamental form of the streamfunction equation on the blade-to-blade surface in (x^3, x^2) co-ordinates may be written as[1-5]

$$A_{10}\frac{\partial^2\psi}{(\partial x^2)^2} + A_{20}\frac{\partial^2\psi}{\partial x^2\partial x^3} + A_{30}\frac{\partial^2\psi}{(\partial x^3)^2} + A_{40}\frac{\partial\psi}{\partial x^2} + A_{50}\frac{\partial\psi}{\partial x^3} = B_0 \tag{1}$$

or

$$\frac{\partial}{\partial x^2}\left(A_{10}\frac{\partial\psi}{\partial x^2} + \frac{A_{20}}{2}\frac{\partial\psi}{\partial x^3}\right) + \frac{\partial}{\partial x^3}\left(A_{30}\frac{\partial\psi}{\partial x^3} + \frac{A_{20}}{2}\frac{\partial\psi}{\partial x^2}\right) = B_0, \tag{2}$$

where

$$\begin{aligned} &A_{10} = \sqrt{g_{33}}/(\rho f\sqrt{g_{22}}), \qquad A_{20} = -2\cos\theta/(\rho f), \qquad f = \tau\sin\theta,\\ &A_{30} = \sqrt{g_{22}}/(\rho f\sqrt{g_{33}}), \qquad A_{40} = \partial A_{10}/\partial x^2 + 0{\cdot}5\partial A_{20}/\partial x^3,\\ &A_{50} = \partial A_{30}/\partial x^3 + 0{\cdot}5\partial A_{20}/\partial x^2, \qquad (3)\\ &B_0 = (\sqrt{g_{33}}/W^3)\,(\partial I/\partial x^2 - T\partial S/\partial x^2 - 2\sqrt{g_{22}}\,W^3\Omega\sin\theta\sin\sigma), \qquad W^3 = \sqrt{g_{33}}\,w^3. \end{aligned}$$

Here w^3 and W^3 are respectively the contravariant component and the contravariant physical component of the relative velocity vector in the x^3-direction, g_{33} is the covariant metric tensor, I is the relative stagnation rothalpy of unit mass of gas and τ denotes the normal distance between two adjacent blade-to-blade surfaces, (its value is known in the present study). For transonic flow it can be shown that equation (2) is a mixed-type equation; that is, in the subsonic region it is an elliptic equation but in the supersonic region it is a hyperbolic equation. In order to introduce the necessary artificial viscosity to ensure stability and the capture of a shock wave, the density in equation (2) must be replaced by the corresponding artificial density $\tilde{\rho}$ (e.g. see Reference 6). Therefore the principal equation in the streamfunction can be written in the following form:

$$\frac{\partial}{\partial x^2}\left(\frac{A_{10}^*}{\tilde{\rho}}\frac{\partial\psi}{\partial x^2} + \frac{A_{20}^*}{2\tilde{\rho}}\frac{\partial\psi}{\partial x^3}\right) + \frac{\partial}{\partial x^3}\left(\frac{A_{30}^*}{\tilde{\rho}}\frac{\partial\psi}{\partial x^3} + \frac{A_{20}^*}{2\tilde{\rho}}\frac{\partial\psi}{\partial x^2}\right) = B_0, \tag{4}$$

where

$$A_{10}^{*} = A_{10}\rho, \qquad A_{20}^{*} = A_{20}\rho, \qquad A_{30}^{*} = A_{30}\rho.$$

DISCRETIZATION AND STONE'S SIP

Standard finite differences are used in discretizing equation (4), namely central differencing everywhere, leading to a large system of non-linear algebraic equations in the unknown streamfunction values at the grid points. At each interior point (i, j) the algebraic equation can be put in compact form as follows:

$$\hat{B}_{1_{i,j}}^{(n)} \xi_{i-1,j}^{(n+1)} + \hat{B}_{2_{i,j}}^{(n)} \xi_{i,j}^{(n+1)} + \hat{B}_{3_{i,j}}^{(n)} \xi_{i+1,j}^{(n+1)} + \hat{B}_{5_{i,j}}^{(n)} \xi_{i,j-1}^{(n+1)} + \hat{B}_{8_{i,j}}^{(n)} \xi_{i,j+1}^{(n+1)} = \hat{R}_{i,j}^{(n)}, \tag{5}$$

where $\xi^{(n+1} \equiv \psi^{(n+1)} - \psi^{(n)}$ and $\hat{R}^{(n)}$ is the residual at iteration level n. The matrix form can be written as:

$$[\hat{\mathbf{B}}]^{(n)} \{\xi\}^{(n+1)} = \{\hat{\mathbf{R}}\}^{(n)}. \tag{6}$$

A direct inversion of the five-point operator is not economical, therefore the resulting five-diagonal system of equations is solved by using Stone's strongly implicit procedure (SIP). Stone's auxiliary matrix $[\mathbf{B}']$ can be put in compact form as follows:[7]

$$[\mathbf{B}'] = \begin{bmatrix} & & & & & & & & \\ & & & & & & & & \\ & & & & & & & & \\ & & & & & & & & \\ & & & & & & & & \\ & & & & & & & & \\ & & & & & & & & \\ & & & & & & & & \\ & & & & & & & & \end{bmatrix} \tag{7}$$

Here α is a sequence of constants given by

$$\alpha_l = 1 - (1 - \alpha_{\max})^{l/(N-1)} \quad (l = 0, 1, 2, \ldots, N-1). \tag{7a}$$

In equation (7a), N and $\alpha_{\max}$ are user-specified constants. In equation (7), the subscript of α_l is omitted. It is a relaxation factor cyclically varied between the limits $0 \leqslant \alpha \leqslant \alpha_{\max} < 1$ during iterations. The numerical molecule associated with the matrix $[\hat{\mathbf{B}} + \mathbf{B}']$ is shown schematically in Figure 2.

Using the above definitions, equation (6) can be put in the following form:

$$[\hat{\mathbf{B}} + \mathbf{B}']^{(n)} \{\xi\}^{(n+1)} = \{\hat{\mathbf{R}}\}^{(n)}. \tag{8}$$

Replacing $[\hat{\mathbf{B}} + \mathbf{B}']$ by $\mathbf{LU}$ results in

$$\mathbf{LU}\{\xi\}^{(n+1)} = \{\hat{\mathbf{R}}\}^{(n)} \tag{9}$$

or

$$(a'_{i,j} E_{x^3}^{-} + b'_{i,j} E_{x^2}^{-} + C'_{i,j})^{(n)} (1 + d'_{i,j} E_{x^2}^{+} + e'_{i,j} E_{x^3}^{+})^{(n)} \xi_{i,j}^{(n+1)} = \hat{R}_{i,j}^{(n)}, \tag{10}$$

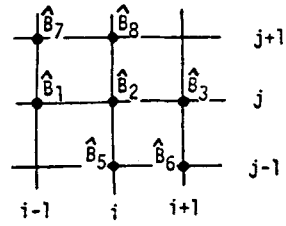

Figure 2. Numerical molecule associated with matrix $[\hat{\mathbf{B}} + \mathbf{B}']$

where $E^{\pm}$ is a shift operator, i.e.

$$E_{x^3}^{\pm}\,\xi_{ij}^{(n+1)} \equiv \xi_{i\pm1,j}^{(n+1)}, \tag{11a}$$

$$E_{x^2}^{\pm}\,\xi_{ij}^{(n+1)} \equiv \xi_{i,j\pm1}^{(n+1)}, \tag{11b}$$

$$a_{i,j}'^{(n)} = \hat{B}_{1_{i,j}}^{(n)}/(1 + \alpha d_{i-1,j}'^{(n)}), \tag{11c}$$

$$b_{i,j}'^{(n)} = \hat{B}_{5_{i,j}}^{(n)}/(1 + \alpha e_{i,j-1}'^{(n)}), \tag{11d}$$

$$C_{i,j}'^{(n)} = \hat{B}_{2_{i,j}}^{(n)} + (\alpha e_{i,j-1}'^{(n)} - d_{i,j-1}'^{(n)})\,b_{i,j}'^{(n)} + (\alpha d_{i-1,j}'^{(n)} - e_{i-1,j}'^{(n)})\,a_{i,j}'^{(n)}, \tag{11e}$$

$$d_{i,j}'^{(n)} = (\hat{B}_{8_{i,j}}^{(n)} - \alpha a_{i,j}'^{(n)}\,d_{i-1,j}'^{(n)})/C_{i,j}'^{(n)}, \tag{11f}$$

$$e_{i,j}'^{(n)} = (\hat{B}_{3_{i,j}}^{(n)} - \alpha b_{i,j}'^{(n)}\,e_{i,j-1}'^{(n)})/c_{i,j}'^{(n)}. \tag{11g}$$

NEW APPROACH AND SYMMETRIC AUXILIARY MATRIX

If we express the matrix $[\hat{\mathbf{B}}]$ as

$$[\hat{\mathbf{B}}] = \tfrac{1}{2}([\hat{\mathbf{B}}] + [\hat{\mathbf{B}}]^{\mathrm{T}}) + \tfrac{1}{2}([\hat{\mathbf{B}}] - [\hat{\mathbf{B}}]^{\mathrm{T}}) \equiv [\mathbf{B}] + [\bar{\mathbf{B}}], \tag{12}$$

where $[\mathbf{B}] \equiv \frac{1}{2}([\hat{\mathbf{B}}] + [\hat{\mathbf{B}}]^{\mathrm{T}})$, it is a symmetric matrix and $[\bar{\mathbf{B}}]$ is non-symmetric. Let

$$\{\mathbf{R}\}^{(n)} \equiv \{\hat{\mathbf{R}}\}^{(n)} - [\bar{\mathbf{B}}]^{(n)}\{\xi\}^{(n)}. \tag{13}$$

Then equation (6) becomes

$$[\mathbf{B}]^{(n)}\{\xi\}^{(n+1)} = \{\mathbf{R}\}^{(n)} \tag{14}$$

or

$$B_{1_{i,j}}^{(n)}\xi_{i-1,j}^{(n+1)} + B_{2_{i,j}}^{(n)}\xi_{i,j}^{(n+1)} + B_{3_{i,j}}^{(n)}\xi_{i+1,j}^{(n+1)} + B_{5_{i,j}}^{(n)}\xi_{i,j-1}^{(n+1)} + B_{8_{i,j}}^{(n)}\xi_{i,j+1}^{(n+1)} = R_{i,j}^{(n)}. \tag{15}$$

The coefficient matrix $[\mathbf{B}]$ and the numerical molecule associated with it are shown in Figure 3.

As a starting point in our study of the symmetric auxiliary matrix, let us consider any symmetric matrix $[\mathbf{A}]$ and its numerical molecule (see Figure 4). Clearly, the basic properties of the matrix $[\mathbf{A}]$ are given by

$$\begin{aligned}(\mathbf{A}_1)_{i,j} &= (\mathbf{A}_7)_{i,j-1}\\ (\mathbf{A}_2)_{i,j} &= (\mathbf{A}_6)_{i+1,j-1}\\ (\mathbf{A}_3)_{i,j} &= (\mathbf{A}_5)_{i-1,j}\end{aligned} \tag{16}$$

It is important to note that this notation does not conform to standard matrix notation; the subscript (i, j) refers to the grid system used in setting up the difference equations rather than to the location within the matrix. In the present study we present a new symmetric auxiliary matrix.

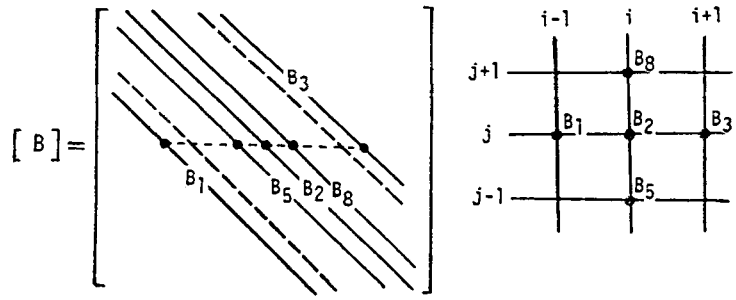

Figure 3. Matrix [**B**] and its numerical molecule

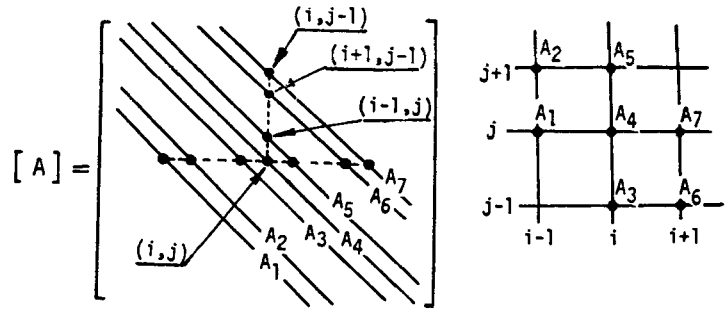

Figure 4. Matrix [*A*] and its numerical molecule

This matrix is defined as follows:

$$[\tilde{\mathbf{B}}] = \begin{bmatrix} & & & & & & \\ & & & & & & \\ & & & & & & \\ & & & & & & \\ & & & & & & \\ & & & & & & \\ & & & & & & \end{bmatrix} \tag{17}$$

It satisfies the properties of (16). In equation (17) the coefficients $a_{i,j}$, $b_{i,j}$, $c_{i,j}$, etc. may be determined by the following relationships:

$$a_{i,j} = B_{1_{i,j}} - \alpha b_{i,j-1} e_{i-1,j-1}, \tag{18a}$$

$$b_{i,j} = B_{5_{i,j}} - \alpha a_{i-1,j} d_{i-1,j-1}, \tag{18b}$$

$$C_{i,j} = B_{2_{i,j}} + \alpha(a_{i-1,j} d_{i-1,j-1} + b_{i,j-1} e_{i-1,j-1}) - a_{i,j} e_{i,j-1} - b_{i,j} d_{i-1,j}, \tag{18c}$$

$$d_{i,j} = (B_{8_{i,j}} - \alpha a_{i,j} d_{i,j-1})/C_{i,j}, \tag{18d}$$

$$e_{i,j} = (B_{3_{i,j}} - \alpha b_{i,j} e_{i-1,j})/C_{i,j}. \tag{18e}$$

Here $\alpha = 1$ is chosen in the present investigation. Therefore the matrix $[\tilde{\mathbf{B}}]$ is a real, symmetric and positive definite matrix. By using factorization techniques, the matrix $[\mathbf{B} + \tilde{\mathbf{B}}]$ has the LU decomposition, i.e.

$$\mathbf{L} = \begin{bmatrix} & & & & \\ & c_{i,j-1} & & & \\ & b_{i+1,j-1} & & & \\ & m & & & \\ & & & c_{i,j} & \\ & a_{i,j} & b_{i,j} & & \\ & & & & \end{bmatrix},$$

$$\mathbf{U} = \begin{bmatrix} & & & & \\ 1 & d_{i,j-1} & e_{i,j-1} & & \\ & m & & & \\ & & d_{i-1,j} & & \\ & & 1 & d_{i,j} & e_{i,j} \\ & & & & \end{bmatrix},$$

where the coefficients $a_{i,j}$, $b_{i,j}$, etc. are defined by the relationships (18)

The matrix $\mathbf{L}$ has non-zero elements in the diagonals corresponding to the $\mathbf{B}_1$, $\mathbf{B}_5$ and $\mathbf{B}_2$ diagonals of the matrix $[\mathbf{B}]$ shown in Figure 3. The matrix $\mathbf{U}$ has non-zero elements in the diagonals corresponding to $\mathbf{B}_2$, $\mathbf{B}_8$ and $\mathbf{B}_3$, with those corresponding to $\mathbf{B}_2$, the principal diagonal, being everywhere equal to unity. Let $\mathbf{D} \equiv \text{diag}(C_{i,j})$ be the diagonal matrix whose diagonal entries are $c_{i,j}$; then

$$\mathbf{L} = \mathbf{U}^{\mathrm{T}}\mathbf{D}, \tag{19}$$

where $\mathbf{U}^{\mathrm{T}}$ is the transpose of $\mathbf{U}$. Therefore

$$[\mathbf{B} + \tilde{\mathbf{B}}] = \mathbf{LU} = \mathbf{U}^{\mathrm{T}}\mathbf{DU} = (\mathrm{diag}(\sqrt{C_{i,j}})\mathbf{U})^{\mathrm{T}}\,(\mathrm{diag}(\sqrt{C_{i,j}})\mathbf{U}) \equiv \mathbf{N}^{\mathrm{T}}\mathbf{N}. \tag{20}$$

The matrix $[\mathbf{B} + \tilde{\mathbf{B}}]$ is a positive definite matrix; if $[\mathbf{B}]$ is symmetric, then $[\mathbf{B} + \tilde{\mathbf{B}}]$ is symmetric too.

CONVERGENCE PROPERTIES OF THE ITERATIVE SCHEME

Let

$$\varepsilon^{(n)} \equiv \psi^{(n)} - \psi \tag{21}$$

and consider the iterative scheme

$$\varepsilon^{(n)} = \mathbf{M}_{\omega}\varepsilon^{(n-1)}, \tag{22}$$

$$\mathbf{M}_{\omega} \equiv \mathbf{I} - \omega(\mathbf{B} + \tilde{\mathbf{B}})^{-1}\mathbf{B}, \tag{23}$$

$$\mathbf{Q} \equiv (\mathbf{B} + \tilde{\mathbf{B}})^{-1}\mathbf{B}, \tag{24}$$

where $\mathbf{I}$ is the identity matrix and $\varepsilon^{(n)}$ is the error vector for the nth iterate. As we know, the error vectors $\varepsilon^{(n)}$ of the iterative methods tend to the zero vector if and only if the spectral radius $\rho(\mathbf{M}_{\omega})$ is less than unity. Clearly, if the matrices $[\mathbf{B}]$ and $[\mathbf{B} + \tilde{\mathbf{B}}]$ are positive definite matrices and $[\mathbf{B} + \tilde{\mathbf{B}}]$ is non-singular, then $(\mathbf{B} + \mathbf{B})^{-1}\mathbf{B}$ is a positive definite matrix too and thus its eigenvalues are positive real numbers. If ω satisfies

$$0 < \omega < 2/\lambda_{\max}[\mathbf{Q}], \tag{25}$$

then for all k,

$$|\lambda_k[\mathbf{I} - \omega\mathbf{Q}]| < 1, \tag{26}$$

where $\lambda_k[\mathbf{P}]$ is the eigenvalue of index k associated with the matrix $\mathbf{P}$; $\lambda_{\max}[\mathbf{Q}]$ represents the maximum eigenvalue among $\lambda_1[\mathbf{Q}], \lambda_2[\mathbf{Q}], \ldots, \lambda_k[\mathbf{Q}], \ldots$. In other words, the spectral radius $\rho(\mathbf{M}_{\omega})$ is less than unity when ω satisfies equation (25). Then the iterative procedure tend to the zero error vector, i.e. the scheme is convergent.

The optimum relaxation factor may be determined as follows:

$$\omega_{\mathrm{opt}} = \frac{2}{\lambda_{\max}[\mathbf{Q}] + \lambda_{\min}[\mathbf{Q}]}. \tag{27}$$

It may be noted that the value of ω_{opt} is not sensitive to the computational results, so that the non-optimal relaxation factor (i.e. the iterative parameter ω) is used in the following calculations.

NUMERICAL SOLUTION PROCEDURES

The solution procedure consists of two steps, namely:

step 1

$$a_{i,j}^{(n)} f_{i,j-1}^{(n+1)} + b_{i,j}^{(n)} f_{i-1,j}^{(n+1)} + C_{i,j}^{(n)} f_{i,j}^{(n+1)} = R_{i,j}^{(n)}, \tag{28}$$

step 2

$$\xi_{i,j}^{(n+1)} + d_{i,j}^{(n)}\xi_{i+1,j}^{(n+1)} + e_{i,j}^{(n)}\xi_{i,j+1}^{(n+1)} = f_{i,j}^{(n+1)}, \tag{29}$$

where $f_{i,j}^{(n+1)}$ is an intermediate result stored at each mesh point. In order to close the system, the $f_{i,j}^{(n+1)}$ and $\xi_{i,j}^{(n+1)}$ are set to zero on whole boundaries.

By using a first-order partial differential equation (PDE) for the density derived from the continuity equation, the momentum equation and the energy equation,[5] the density field is obtained. With this method, the problem of non-uniqueness of the density in the traditional streamfunction method is avoided.

NUMERICAL RESULTS

The method described above has been used to calculate a number of blade cascades. The first test example is computation of a $T_1 - (18A_6I_{4b})08$ cascade with a 50 × 11 mesh. The inlet Mach number is 0·658 and the inlet angle 30°. The relative pitch is $\bar{t} = 1{\cdot}5$. If a fall in the residual by three orders of magnitude is taken to be the convergence criterion, convergence in this case is achieved in approximately 36 iterations. The original SIP reaches this level in 48 iterations. In this case the flow field is a simple subsonic flow and the convergence speed is quite fast.The velocity distribution obtained is compared with the experimental data[8] in Figure 5. The agreement is very good. In the calculation procedure the relaxation factor ω is chosen as 0·6.

The second example is for a DCA 2-8-10 cascade with a 50 × 11 mesh. The inlet Mach number is 1·03 and the inlet angle 61·8°. The relative pitch is $\bar{t} = 0{\cdot}85$ and P_2/P_1 is chosen as 1·29. In this case the flow field is a transonic flow. On the basis of a three-order-of-magnitude fall in maximum residual, the improved SIP and original SIP reach this level in 77 and 93 iterations respectively. In

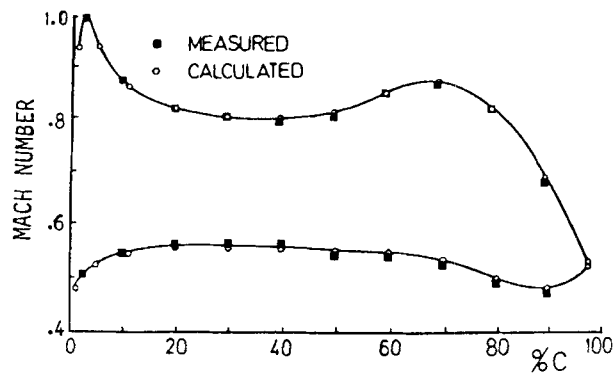

Figure 5. Surface Mach number comparison

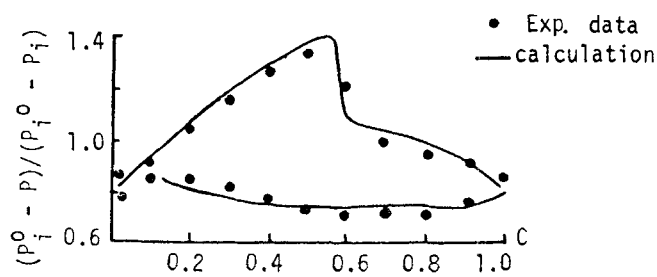

Figure 6. Pressure distribution around blade and comparison with experimental data

Figure 6 the pressure distributions around the blade obtained by the present method are shown. The results of the calculations are seen to agree with the experimental data[9] fairly well. Note that the axial velocity density ratio Ω' must be considered. In the calculation procedure a value of 1·05 is taken for Ω'.

In Reference 10 the flow field within a transonic axial compressor rotor designed for a total pressure ratio of 1·51 at a relative tip Mach number of 1·4 and 100% speed with a mass flow of 16·8 $kg\,s^{-1}$ has been measured by a laser velocimeter. There are four distinctly different types of

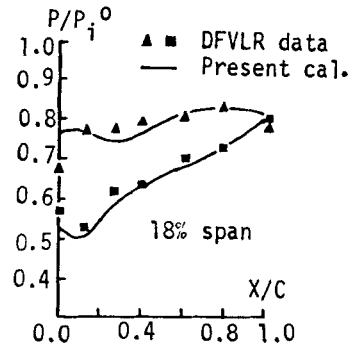

Figure 7. Surface pressure distributions (18% span)

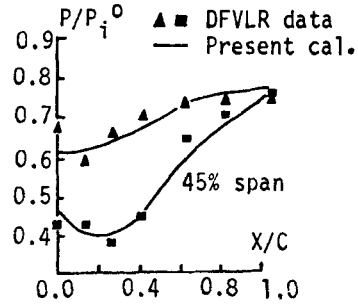

Figure 8. Surface pressure distributions (45% span)

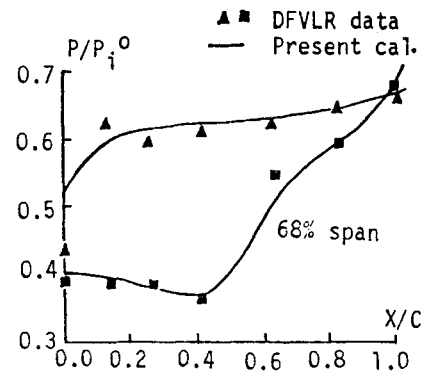

Figure 9. Surface pressure distributions (68% span)

flow field existing simultaneously along the span. These are: (1) a subsonic inlet with a local supersonic region at 18% blade height; (2) a slightly supersonic inlet with a detached shock at 45% blade height; (3) a moderate supersonic condition with a strong attached shock at 68% blade height; (4) a higher supersonic inlet Mach number with a weak oblique-normal shock at 89% blade height.

In this paper the present algorithm was applied to calculate the above four flow fields. Figure 7 defines the surface pressure distributions at 18% span; the computed boundary conditions on the section are inlet Mach number $M_1 = 0{\cdot}922$, relative air angle measured from the tangential $\beta_1 = 35{\cdot}41$, $P_2/P_1 = 1{\cdot}438$. Figure 8 defines the surface pressure distributions at 45% span; the computed boundary conditions are $M_1 = 1{\cdot}086$, $\beta_1 = 31{\cdot}59$, $P_2/P_1 = 1{\cdot}558$. The surface pressure

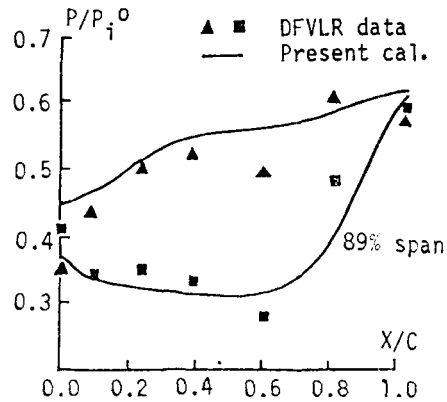

Figure 10. Surface pressure distributions (89% span)

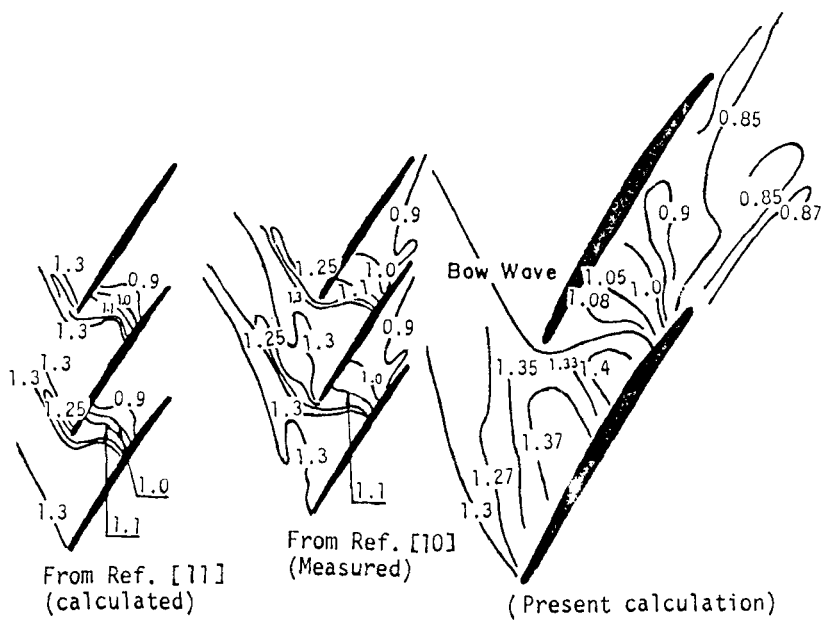

Figure 11. Mach number contours (89% span)

distributions at 68% span are shown in Figure 9; the computed boundary conditions are $M_1 = 1{\cdot}217$, $\beta_1 = 28{\cdot}08$, $P_2/P_1 = 1{\cdot}615$. Figure 10 defines the surface pressure distributions at 89% span; the boundary conditions are $M_1 = 1{\cdot}307$, $\beta_1 = 24{\cdot}04$, $P_2/P_1 = 1{\cdot}63$.

It is clear from these figures that the computed and measured surface pressure distributions are essentially the same. In our computations, converged surface pressure distributions were obtained in about 72, 81, 118 and 136 iterations for the above four sections respectively. The results indicate that the present algorithm converges very rapidly to a reasonably accurate solution. Figure 11 defines the flow field at 89% span. The calculated result agrees with the experimental data[10] fairly well.

It should be noted that the preceding results, which are obtained at different spanwise stations using the blade-to-blade surface calculation, are based on the geometrical shape of the blade-to-blade surface and the distributions of normal thickness of the surface. In the present study the shape of the surface and the distributions of τ are known; they are derived from through-flow calculations on the hub-to-tip mean stream surface located somewhere in the midpart of the flow passage. The problem of the through-flow calculations will not be pursued here.

CONCLUDING REMARKS

An algorithm has been developed that is capable of treating practical transonic cascade flow. Since the auxiliary matrix $[\tilde{\mathbf{B}}]$ is positive definite and symmetric and the coefficient matrix $[\mathbf{B}]$ of the difference equation for the streamfunction equation is symmetric, we are ensured of obtaining reliable converged solutions. For an appropriate choice of iterative parameter ω, the rate of convergence of the new improved SIP should be faster than that of the original SIP. The numerical results suggest that the present algorithm is efficient and robust for calculating transonic cascade flow fields.

APPENDIX: NOMENCLATURE

$A_{10}, A_{20}, \ldots, A_{50}$	coefficients of streamfunction equation
B_0	right-hand-side term of equations (1), (2) and (4)
$[\mathbf{B}']$	Stone's auxiliary matrix
$[\tilde{\mathbf{B}}]$	auxiliary matrix in present scheme
g_{ij}	covariant metric tensor of x^i co-ordinate system
h	enthalpy of unit mass of gas
I	relative stagnation rothalpy, $[h - (\Omega r)^2/2] + (W)^2/2$
ι	meridional co-ordinate for blade-to-blade surface of revolution
(r, ϕ, z)	cylindrical co-ordinate system
S	entropy of unit mass of gas
T	absolute temperature (K)
W	relative velocity of gas
x^i	(x^3, x^2, x^1) curvilinear co-ordinates
Z	co-ordinate along machine axis
ρ	density of gas
$\tilde{\rho}$	artificial density
σ	angle between Z and ι
θ	angle between x^3 and x^2 co-ordinate lines (angle included by x^3 and x^2 co-ordinate lines)

ψ	streamfunction
ω	relaxation factor
Ω	angular velocity of rotating rotor
Ω'	axial velocity density ratio

REFERENCES

1. C.-H. Wu, 'Three-dimensional turbomachine flow equation expressed with respect to non-orthogonal curvilinear coordinates and methods of solution', *3rd Int. Symp. on Air Breathing Engines*, Munich, 1976.
2. N.-X. Chen, 'Some problems in viscous gas flow in turbomachinery—viscous and heat-transfer terms and methods for solution of basic equations', *Sci. Sinica* (*Ser.* A), (10), 956–966 (1983).
3. N.-X. Chen and F.-X. Zhang, 'A comparison between full and simplified Navier–Stokes equation solutions for rotating blade cascade flow on s_1 stream surface of revolution', *ASME Paper 85-GT-4*, 1985.
4. N.-X. Chen W.-H. Li, 'A new method for solving aerodynamic hybrid problem of profile cascade on S_1 stream surface of revolution by employing streamfunction equation expressed with non-orthogonal co-ordinate system', *Int. J. numer. methods eng.*, **22,** 465–479 (1986).
5. B.-G. Wang, 'An iterative algorithm between stream function and density for transonic cascade flow', *J. Propulsion Power*, **2,** 259–265 (1986); also in *AIAA Paper 85–1594*, 1985.
6. M. Hafez and D. Lovell, 'Numerical solution of transonic stream function equation', *AIAA J.*, **21,** 327–335 (1983).
7. H. L. Stone, 'Iterative solution of implicit approximations of multidimensional partial differential equations, *SIAM J. Numer. Anal.*, **5,** 530–558 (1968).
8. M. Savage, R. Felix and J. Emery, 'High-speed cascade tests of a blade section designed for typical hub conditions of high-flow transonic rotors', *NACA RM L55F07*, 1955.
9. H. Starken, 'Untersuchung der Stromung in Ebenen Uberschall-Verzogerung Gittern', *DLR FB 71–99*, 1971.
10. R. J. Dunker, P. E. Strinning and H. B. Weyer, 'Experimental study of the flow field within a transonic axial compressor rotor by laser velocimetry and comparison with through-flow calculations', *Trans. ASME, J. Eng. Power*, **100,** 279–286 (1978).
11. P. W. McDonald, C. R. Bolt, R. J. Dunker and H. B. Weyer, 'A comparison between measured and computed flow fields in a transonic compressor rotor', *Trans. ASME, J. Eng. Power*, **102,** 883–889 (1980).